Hindawi

Research Article

Experiment and Improvement Mechanism Analysis on the Mechanical Properties of Improved Chlorine Saline Soil

Semaierjiang Maimaitiyusupu [iD],[1,2,3] **Cheng Zhao,**[3] **and Shichao Tao**[2]

[1]*College of Water Conservancy and Hydropower Engineering, Hohai University, Nanjing 210098, China*
[2]*College of Civil Engineering, Kashi University, Kashgar 844006, China*
[3]*Key Laboratory of Geotechnical and Underground Engineering of the Ministry of Education, Tongji University, Shanghai 200092, China*

Correspondence should be addressed to Semaierjiang Maimaitiyusupu; samarjan@hhu.edu.cn

Semaierjiang Maimaitiyusupu and Cheng Zhao contributed equally to this work.

Chlorine saline soil has adverse engineering geology such as dissolution, collapse, and pulping, the recycling of saline soil in subgrade treatment is of great research significance. First, the unconfined compressive strength (UCS) test was conducted using an orthogonal test design, and the optimal ratios of salt content, cement content, lime content, fiber content, and fiber length were determined. Second, the cyclic loading (CL) test was conducted using an orthogonal test design, and the influence of five factors, including freeze–thaw (FT) times, CL times, stress level (SL), amplitude, and frequency, on peak intensity, peak strain, and cumulative strain under FT cycles and natural air-drying (A-D) conditions were determined. Finally, the improvement mechanism of the above inorganic materials was microscopically analyzed by scanning electron microscope-energy dispersive spectrometer and X-ray diffraction tests. The UCS test results show that the improving effect of the optimal ratio for chlorine saline soil was best when the optimal ratio values were 3% (salt content), 8% (cement content), 12% (lime content), 0.2% (fiber content), and 18 mm (fiber length). CL test results show that with the increase in natural A-D time, it was found that the FT number and SL have significant effects on the strength, the number of FT times and cycle times have significant effects on the deformation, and the frequency and cycle times have significant effects on the cumulative deformation. From the microstructure analysis, the improvement mechanism is mainly the filling of pores and linking particles by water-hard gels and gas rigid gels to make the microstructure dense, effectively reduce pores, and effectively improve the engineering characteristics of chlorine saline soil. The results of this study provide a scientific basis for the engineering design of subgrade in arid areas and the in situ recycling of saline soil.

1. Introduction

The arid climate, sparse rain, high evaporation rate, and low-lying topography of the southern Xinjiang region have led to the formation of vast tracts of saline soil. Under the conditions of the natural environment, the migration of water and salt in saline soil and its consequent unfavorable engineering geological characteristics have significantly impacted the reliable and stable functioning of engineering facilities [1, 2]. As such, research on the improved recycling of saline soil and the physical and mechanical characteristics of improved saline soil

under different environmental conditions has considerable theoretical significance and engineering application value in the practice of traffic engineering construction.

At present, numerous scholars have reported notable results on the improvement of various types of soil. Rajasekaran [3] investigated the treatment method of calcareous aluminite lime to treat clays and suggested that stabilization techniques should be used with caution in sulfate-rich clays. Cheng et al. [4] explored the solidification of chlorine saline soil of slag and found that sodium chloride was the main cause affecting the strength of slag solidified chlorine saline soil. The relationship

between strength increase and chlorine content was also identified. Shen et al. [5] proposed a composite slag curing agent composed of slag, quicklime, water glass, and gypsum powder. Liu et al. [6] proposed a method for curing coastal saline soil with slag composite cementitious material as curing agent. Qin et al. [7] investigated the effects of lime–lime ratio, lime content, age, compression degree, and salt content on the compressive strength of solidified coastal saline soil. Liu [8] conducted research on the strength deformation and microstructure of improved soil of slag cementitious materials. Zhu et al. [9] proposed a new water-based polymer that can improve the strength, water stability, and dry–wet cycle resistance of saline soil. After studying the freeze–thaw (FT) resistance of stable sulfate saline soil, Zhou et al. [10] proposed that a high proportion of stabilizers can improve the FT resistance of stable soil. Zhang et al. [11] employed polypropylene fiber to reinforce red clay and investigate its strength and failure characteristics. Under different fiber contents, lime contents, and fiber strength conditions, Wang [12] explored the curing effect of saline soil and proposed the optimal lime–fiber ratio. Yu and Sun [13] studied the composite improvement of saline soil with lime cement based on the compressive strength of unconfined saturated water and recommended the improvement scheme of 5% lime + 3% cement considering the strength and economy. LÜ et al. [14–16] heated and modified water glass, and the effect of modified water glass, lime, and fly ash was improved by means of strength, X-ray, scanning electron microscope (SEM), and nuclear magnetic resonance testing. Xing et al. [17] investigated the effect of alkali activation on the mechanical properties of saline soil, and $Ca(OH)_2$ and $NaOH$ as alkaline activators were found to significantly improve the unconfined compressive strength (UCS) of saline soil. Wang et al. [18] investigated the effect of alkali-activated steel slag on the mechanical properties of saline soil, and the compressive strength of the soil was found to be significantly improved when the incorporation amount of alkali-activated steel slag exceeded 15%. Chai et al. [19–23] explored the effect of salt content on the strength, compaction, and microstructure of lime-solidified coastal saline soil, and proposed the optimal ratio of lime, fly ash, and modified poly (vinyl alcohol) (SH) solid soil agent to solidify coastal saline soil. Wei et al. [24] conducted macroscopic mechanical testing and microscopic analyses on six kinds of stable soils, and the results showed that lime, cement, fly ash, and SH agent could improve the mechanical properties of saline soils. In particular, the strength of SH-stabilized soils was significantly increased after immersion. The described research results reveal the improvement effect and solidification mechanism of various curing agents on soil, but the focus of most research has been on the reinforcement of sulfate saline soil, in addition to the improvement of chlorine saline soil in coastal areas. At present, most of the research results on the reinforcement of chlorine saline soil in arid areas concern superchlorine saline soil. Wang et al. [25] conducted a study exploring the utilization of a chlorine saline soil sand fixation scheme in arid regions. In cases where the chloride ion content was high, water glass was utilized as a curing agent to enhance the sand fixation efficacy. Wang et al. [26] took the superchlorinated saline soil of Charkhan Salt Lake as the research object and used portland cement to improve the

FIGURE 1: Site sampling location.

superchlorinated saline soil. The test results show that a 15% cement content was the optimal mixing ratio for enhancing the properties of the improved Charkhan superchlorine saline soil. Wang et al. [27] used recycled powder, fly ash, and cement to solidify the strength characteristics, microscopic mechanism, and curing mechanism of superchlorine saline soil. Sun et al. [28] took superchlorine saline soil in extremely arid desert areas as the research object, and water glass as the curing agent, when the concentration of water glass was 16% and the content was 18%, the sample strength could reach over 1 MPa. In summary, the existing research results regarding the reinforcement of chlorine saline soil in arid regions are primarily focused on addressing the unique circumstances associated with high salinity content. For saline soils with medium chlorine saline soil in arid areas, the aforementioned improved saline soil scheme needs to be further optimized, and there is a need to verify the adaptability and effectiveness of improved saline soil schemes under complex conditions.

In arid areas with saline soil, using local materials instead of transporting subgrade filler from elsewhere can save construction costs and time. In the present study, based on the described research results, inorganic materials such as cement, lime, water glass, and fiber were used to improve saline soil, and the optimal improvement ratio suitable for the reinforcement of chlorine saline soil in arid areas was proposed. Further investigated the adaptability and effectiveness of the improved saline soil under diverse and complex conditions, including arid environments, FT environments, and cyclic loading (CL). In addition, microscopic analysis was utilized to gain further insight into the improvement mechanism of the optimal mixing ratio. This paper aims to propose an optimal improved ratio for the treatment of chlorine saline soil in arid areas, reveal its micro-improvement mechanism, and provide a theoretical basis for the feasibility of using in situ saline soil to treat subgrade.

2. Test Procedure

2.1. Soil Sample Selection. The soil samples for testing were taken from a certain section from Kashgar to Artush (39°39′27″N, 76°6′48″E), and the on-site sampling points are shown in Figure 1. According to the *Standard for Geotechnical Testing Methods* (*GB/T 50123-2019*) [29], the liquid limit of soil sample is 29%, the plastic limit is 20%, the plasticity index is 9, and the liquid index is 0.54. A plastic chart of the saline soil is shown in Figure 2. A light compaction test was conducted, with
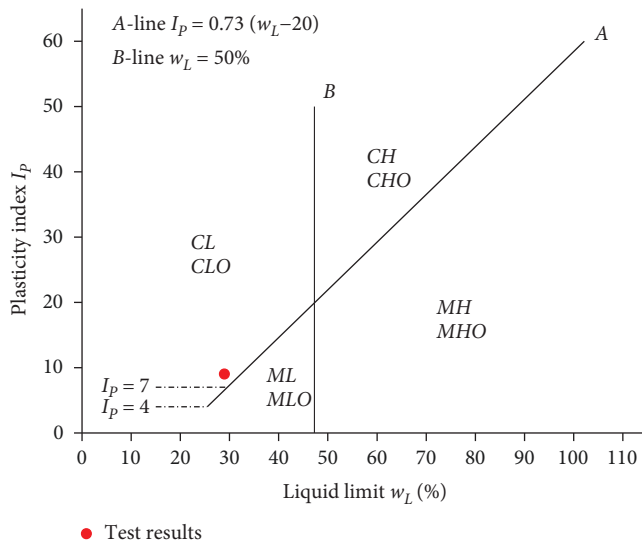
FIGURE 2: Plasticity chart of saline soil.

TABLE 1: Soluble salt content of soil samples.

Depth (m)	Ion content (%)			Total content (%)
	SO_4^{2-}	Cl^{1-}	Na^{1+}	
0.1	0.391	4.892	2.931	8.651
0.4	0.38	2.375	1.188	4.452
0.7	0.391	1.794	0.999	3.556
1.0	0.377	1.531	0.993	3.122

the maximum dry density being 1.66 g/cm^3 and the optimal water content being 19.9%. Chemical analysis provided information on the soil ion content at a depth of 1 m, as shown in Table 1. The surface saline soil had a total salt content of 8.651%, consisting of a SO_4^{2-} content of 0.391% and a Cl^- content of 4.892%. The Cl^- to SO_4^{2-} ratio was 12.51, which exceeds 3. The weighted average salt content within the 1-m range was 4.2%, indicating that the soil belonged to the category of medium chlorine saline soil.

Using the Bettersize2600 laser particle size instrument, the particle size distribution of saline soil was determined using the dry method. The particle size distribution curve is shown in Figure 3. The particles exhibited a specific surface area of 0.5719 m^2/g, with an average surface area diameter of 3.887 μm and an average volume diameter of 22.74 μm. The particle size distribution was characterized by $D_{10} = 1.332\ \mu$m, $D_{30} = 5.027\ \mu$m, and $D_{60} = 20.55\ \mu$m. The coefficient of uniformity (C_u) was 13.317, while the coefficient of curvature (C_c) was 0.692. Based on the aforementioned test results and the plastic chart of saline soil (see Figure 2), the soil could be categorized as a poorly graded clayey silt.

2.2. Test Materials. The test materials included: plain soil, sodium chloride, cement, lime, water glass, and polypropylene fiber. The specific parameters for each material were as follows:

(1) Plain soil: the salt in the saline soil was washed until the salt content met the requirements specified in the Standard for Geotechnical Testing Methods (GB/T 50123-2019) [29].

(2) Sodium chloride: powdered anhydrous sodium chloride was used. The grade was analytical pure, and the effective NaCl content was not less than 99.5%.

(3) Lime: quicklime powder was used. The effective calcium oxide and magnesium oxide content was 60%.

(4) Water glass: in the tests conducted, the water glass liquid had a chemical formula of Na$_2$O·nSiO$_2$, with silica (SiO$_2$) constituting 28.1% and sodium oxide (Na$_2$O) comprising 9% of its composition. The modulus of water glass was 3.12, its concentration ranged from 39° to 40° Bé, and its density was 1.394 g/ml. The water glass used in the tests was diluted with distilled water in a 1 : 1 ratio.

(5) Polypropylene fiber: the fiber utilized in the tests was a bundled monofilament type, with a diameter ranging from 18 to 48 μm and a specific gravity of 0.91. Its tensile strength was greater than 458 MPa, with an elastic modulus greater than 3.5 GPa and a tensile limit greater than 150%. In addition, it exhibited high resistance to acid and alkali and was able to withstand low temperatures. The appropriate selection of fiber type, length, and content significantly improves the UCS of soil [30–32]. The physical and mechanical properties, size (length, diameter), and deviation of the polypropylene fiber selected in this study meet the requirements of the Fiber for Cement Concrete in Highway (JT/T 524-2019) standard [33].

(6) Cement: P·O42.5 grade ordinary portland cement was utilized in the tests, which had a main chemical composition consisting of 57.99% CaO, 24.23% SiO$_2$, 6.11% Al$_2$O$_3$, 2.71% SO$_3$, 2.69% Fe$_2$O$_3$, and 2.45% MgO. The specific surface area of the cement was not less than 300 m^2/kg, the initial setting time was greater than 3 hr, the final setting time was greater than 6 hr, and less than 10 hr. The compressive strengths of 3 and 28 days were not less than 16 and 42.5 MPa, respectively. Good frost resistance, less shrinkage. As an inorganic stabilizer, the cement meets the execution requirements for the use of cement stabilizer in the current Technical Guidelines for the Construction of Highway Roadbases (JTG/T F20-2015) [34].

2.3. Test Methods. Inorganic materials such as cement, lime, water glass, and polypropylene fiber were selected as curing agents to improve saline soil, and the curing effect and mechanism of inorganic materials combined with improved chlorine saline soil were explored. The experiment process involved the following:

(1) Unconfined compressive strength testing (UCS testing). A 250D microcomputer-controlled testing machine was used for UCS testing, with a loading rate of 1 mm/min. Wei et al. [35], Xing et al. [36], and Yu et al. [37] conducted studies aimed at enhancing the engineering characteristics of coastal chlorine saline soil through the use of inorganic materials such as lime (with a content
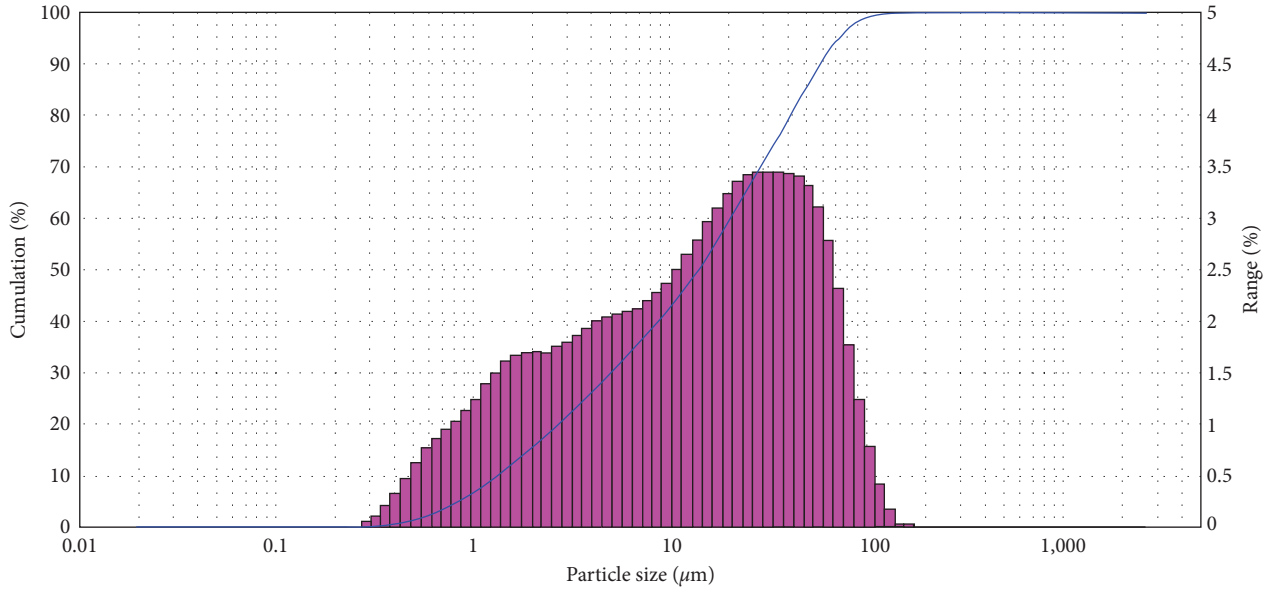
FIGURE 3: Particle size distribution curve of soil sample.

TABLE 2: Orthogonal tests.

Level	A (%)	B (%)	C (%)	D (%)	D (mm)
1	1	2	3	0.1	9
2	3	4	6	0.2	12
3	5	6	9	0.3	15
4	7	8	12	0.4	18

FIGURE 4: Changes in atmospheric temperature for three consecutive years.

ranging from 6% to 14%), cement (with a content ranging from 0% to 9%), and fiber (with a length ranging from 6 to 31 mm and a content ranging from 0% to 0.3%). Based on the aforementioned research results, a five-factor four-level $L_{16}(4^5)$ orthogonal test was designed. Five factors were selected, namely salt content (A), cement content (B), lime content (C), fiber content (D), and fiber length (E). Three samples were taken and the average was calculated as the test result for that group. Through analysis of the test results, the optimal combination of strength for the inorganic materials combined with the improved saline soil was determined. The orthogonal design utilized in the tests is presented in Table 2.

(2) Freeze–thaw testing (F-T testing). According to the optimal combination of strength obtained by the UCS testing, samples were prepared and cured for 28 days under standard conditions. The surface moisture was wiped after curing and sealed with plastic wrap to prevent the water from evaporating, before being immediately placed in a FT cycle test box. The tests were conducted in a TMS 9018-800 frost heave/ FT cycle test chamber. The samples were subjected to FT cycles for 0, 2, 4, and 6 times. The FT cycle was 24 hr, including 12 hr of freeze and 12 hr of thawing. According to the temperature data of the local climate station, through the analysis of the local atmospheric
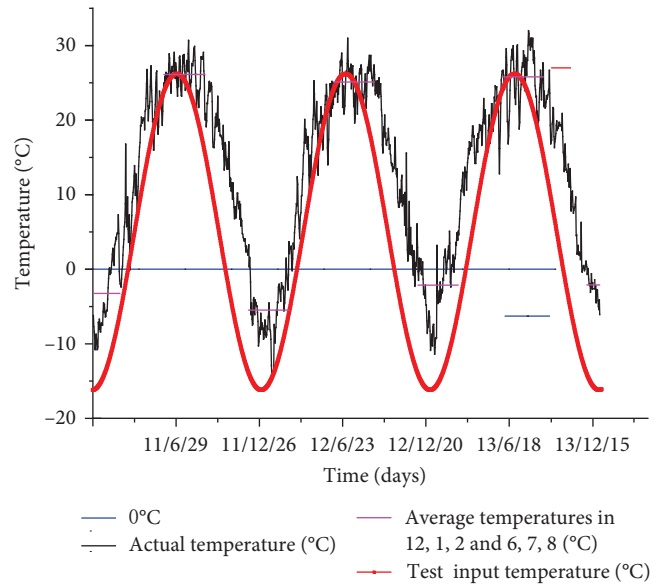
temperature data for three consecutive years, the average atmospheric temperature in June, July, and August was 25.11–26.12°C. The average atmospheric temperature in December, January, and February was −2.14 to −5.48°C. In winter, the low temperature was found to fluctuate greatly, with a low temperature of −14.5°C, and many extreme adverse climates were identified, as shown in Figure 4.

Considering the extremely unfavorable climate, the F-T testing was controlled at −15°C at low temperature and 25°C at high temperature. In the tests, the temperature of the environmental chamber was first adjusted to 5°C, and then
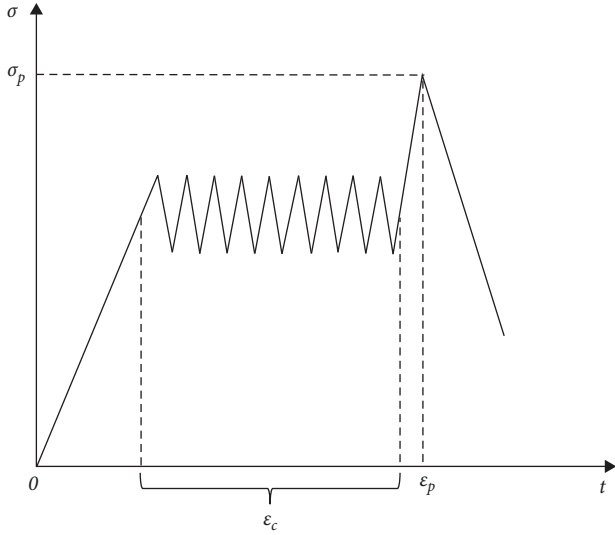
FIGURE 5: Loading methods.

TABLE 3: Cyclic loading orthogonal test protocol.

Level	FT (n)	CL (n)	SL (%)	LA (%)	LF (Hz)
1	0	1,000	40	5	0.1
2	2	2,000	50	10	0.2
3	4	3,000	60	15	0.5
4	6	4,000	70	20	1

the FT cycle was performed. The temperature during the FT cycles was controlled based on a sine wave equation, which can be denoted as follows:

$$T_\alpha = \begin{cases} 5 & t_h \in (0, 24] \\ 20 \sin{(\pi x/12)} + 5 & t_h \in (24, 168], \end{cases} \quad (1)$$

where T_a is the actual input temperature (°C) and t_h is the temperature control time (hr).

(3) Natural air-drying (A-D). Following the 0, 2, 4, and 6 FT tests, the samples were then placed under 30 ± 2°C conditions and allowed to naturally A-D for 0, 7, 14, and 28 days. The samples were utilized in the UCS and CL tests.

(4) Cyclic loading testing (C-L testing). First, the UCS tests were conducted on the samples that were subjected to different FT times and natural A-D days. Based on the aforementioned UCS test results, the initial stress level (SL) and CL amplitude of CL were determined. The test loading step was controlled by the RMT-301's own load CL system, using a sine wave waveform. The loading mode is shown in Figure 5. Second, the five-factor four-level $L_{16}(4^5)$ orthogonal test was used, and five factors such as FT times, CL times, SL, loading amplitude (LA), and loading

frequency (LF) were selected. The orthogonal test design is shown in Table 3.

(5) SEM-EDS (energy dispersive spectrometer) and X-ray diffraction (XRD) testing. Using the Phenom ProX electron microscopy integrated machine, the fractures of the damaged samples taken from the test were scanned at a magnification of 4,000 times, and EDS analysis was performed. The structural morphology, particle arrangement characteristics, and contact mode of the improved saline soil samples were analyzed. The main components and percentage content of hydration products were obtained using the Bruker D8 Advance X-ray diffractometer.

2.4. Sample Preparation. The samples were made in accordance with the *Standard for Geotechnical Testing Methods* (*GB/T 50123-2019*) [29]. According to the optimal water content, maximum dry density, and design ratio (see Table 2), the amounts of plain soil, cement, lime, water glass, and anhydrous sodium chloride required for each specimen were calculated. According to the calculation results of the materials, each material was weighed and mixed evenly, and then the mixture was formed by spraying the test water glass. With a dry density of 1.66 g/cm^3 as the control standard, a cylindrical specimen with a compaction degree of 96% was quickly made by bidirectional static compaction method, and a stable pressure was maintained for 3 min to reduce the rebound of the soil sample.

(1) UCS test samples. The samples were prepared according to the orthogonal test requirements of Table 1. Cylindrical samples with a diameter of 50 mm and a height of 50 mm were made, with a total of 16 groups of 48 samples. After being formed, the samples were cured for 28 days under standard conditions (temperature of 20 ± 2°C, humidity of 95%). On the last day, the samples were immersed in water for 24 hr, and then the UCS testing was conducted.

(2) C-L test samples. The samples were prepared according to the optimal combination of strength obtained by the orthogonal test in Table 1. Cylindrical samples with a diameter of 50 mm and a height of 100 mm were made, with 20 groups of 240 samples. After being formed, the samples were cured for 28 days under standard conditions (temperature of 20 ± 2°C, humidity of 95%), and then FT cycle testing was conducted.

(3) SEM-EDM test samples. SEM test samples were taken from different typical parts of the failure fracture of the specimen. Three sections were taken at the top, middle, and lower positions of the failure samples with a size of about 10×10 mm. Sections were subjected to vacuum sputtering gold spraying before testing, using Phenom ProX and applying the accompanying EDS to selected representative areas.

(4) XRD test samples. The XRD test samples were taken from the broken samples of UCS tests that solidified 28 days, and grounded into a powder. The XRD
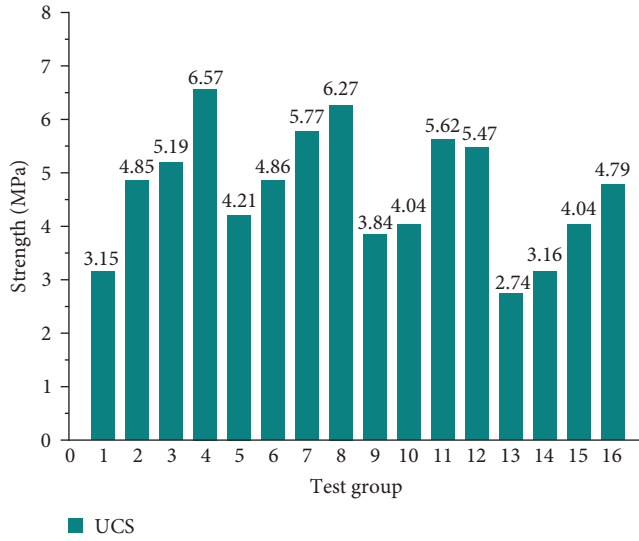
FIGURE 6: Histogram of the results of the UCS test.

TABLE 4: Range analysis results of strength.

K_i	A (%)	B (%)	C (%)	D (%)	E (%)
K_1	4.940	3.485	4.605	4.388	4.375
K_2	5.277	4.228	4.642	4.870	4.813
K_3	4.742	5.155	4.615	4.558	4.565
K_4	3.683	5.775	4.780	4.827	4.890
R	1.594	2.290	0.175	0.482	0.515

TABLE 5: UCS test results.

	UCS (MPa)			
F-T times (n)	A-D for 0 days	A-D for 7 days	A-D for 14 days	A-D for 28 days
0	2.35	3.21	4.09	3.92
2	1.85	2.25	3.50	3.02
4	1.67	1.86	3.42	2.72
6	1.59	1.74	3.33	2.65

pattern analysis was conducted using a Bruker D8 Advance X-ray diffractometer.

3. Test Results and Analysis

3.1. UCS Testing. According to the orthogonal test design (see Table 2), the results of the UCS tests of each group of samples at the age of 28 days are shown in Figure 6.

Table 4 is the range analysis table of evaluation indicators, where K_i $(i = 1, 2…)$ represents the sum of the test results at the i level of a factor, and K_i represents its mean value. R is the range value. Under the condition of 28 days of curing period, the degree of influence of the five factors on the compressive strength was analyzed based on the range difference. A larger R value indicates a greater influence of the corresponding test factors on the test results, while a smaller R value indicates a lower degree of influence. Based on the results of the UCS test, the five factors were found to influence the compressive strength of the 28-day-old specimen in the following order: cement content, salt content, fiber length, fiber content, and lime. Using compressive strength as the evaluation standard, the optimal combination of each factor was determined. The results indicate that the optimal combination was $A_2B_4C_4D_2E_4$, corresponding to a salt content of 3%, cement content of 8%, lime content of 12%, fiber content of 0.2%, and a fiber length of 18 mm. This combination is suitable for the treatment of medium saline soils, according to the engineering classification of saline soils.

3.2. C-L Testing. The samples were prepared based on the optimal combination ratio of strength and were subjected to FT cycles of 0, 2, 4, and 6 times. The samples were then naturally A-D for 0, 7, 14, and 28 days, and underwent UCS testing. The test results are presented in Table 5.

As shown in Figure 7, under the same natural A-D days, the water inside the soil sample underwent frost heaving and thawing contraction as the number of FT cycles increased. Such a

process damaged the internal skeleton of the soil body, resulting in an increase in the internal pores of the sample. As a result, the UCS of the sample gradually decreased. As shown in Figure 8, under the same number of FT cycles, the UCS of the soil sample increased with an increase in the number of natural A-D days. Such findings could be attributed to the evaporation of internal water from the soil sample as it dried, causing the soil to lose water. As the water content decreased, the salt gradually crystallized and precipitated, filling the soil pores. This resulted in an increase in the UCS of the soil sample. When the soil samples were further dried naturally, part of the salt migrated under the action of capillary water and evaporation, and accumulated on the surface of the samples. On the other hand, the salt expansion phenomenon caused shedding and surface destruction of the samples, and the migration of water and salt generated certain pores in the soil, resulting in the reduction of the UCS of the sample, and the whole process exhibited a trend of first increasing and then decreasing.

The selected typical stress–strain curve of C-L testing is presented in Figure 9. As the number of natural A-D days increased, both the peak strength and peak strain of the sample increased to varying degrees. After the stress of the improved saline soil exceeded the peak, the high compressive strength value could still be maintained, and the distribution of fibers in the sample was found to be conducive to the improvement of compressive strength to a certain extent. The addition of fiber not only improved the strength of the sample but also enhanced the deformation performance [38, 39].

According to the results of the CL test of the improved saline soil, the peak strength, peak strain, and cumulative strain values of each group of samples under different test conditions were obtained, as shown in Table 6.

Figure 10 demonstrates that, under the same number of FT cycles, the peak intensity of the CL test corresponding to groups 2, 4, 5, 7, 10, and 13 showed an overall trend of first increasing and then decreasing as the number of natural A-D
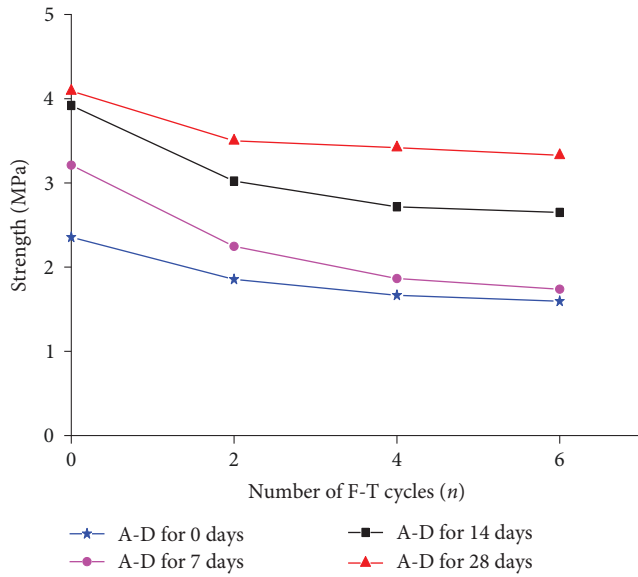
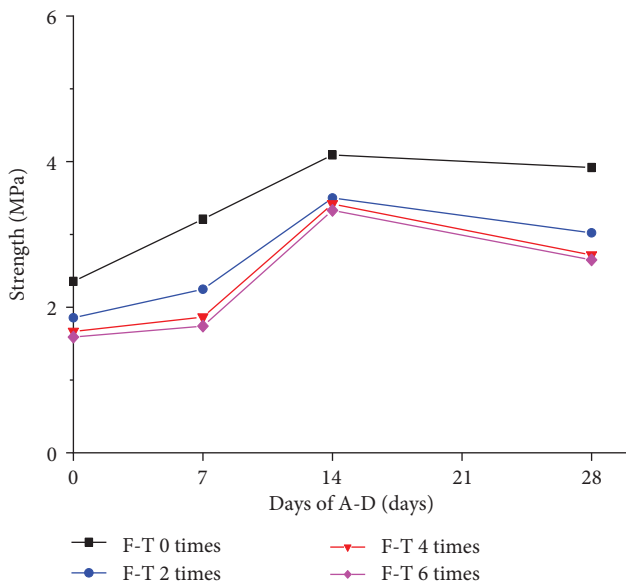FIGURE 7: Relationship between freeze–thaw times and strength.

FIGURE 8: Relationship curve between natural air-drying days and intensity.

FIGURE 9: Stress–strain curve of C-L test.

days increased. The corresponding stress groups were found to be 70% and 50%, respectively. When the SL was 70%, the CL strength initially increased and then decreased, indicating that the SL had a greater influence on the CL strength of the samples than the number of FT cycles or natural A-D times. In other cases, the CL strength basically increased first and then maintained a certain level, with small fluctuations. With the increase in the number of FT cycles, the relationship curve between peak intensity and natural A-D days first increased and then decreased significantly.

Figure 11 demonstrates that the peak strain of the CL test for groups 1, 2, 3, and 4 (corresponding to 0 FT cycles) initially increased and then decreased as the number of natural A-D days increased. As the number of natural A-D days increased,
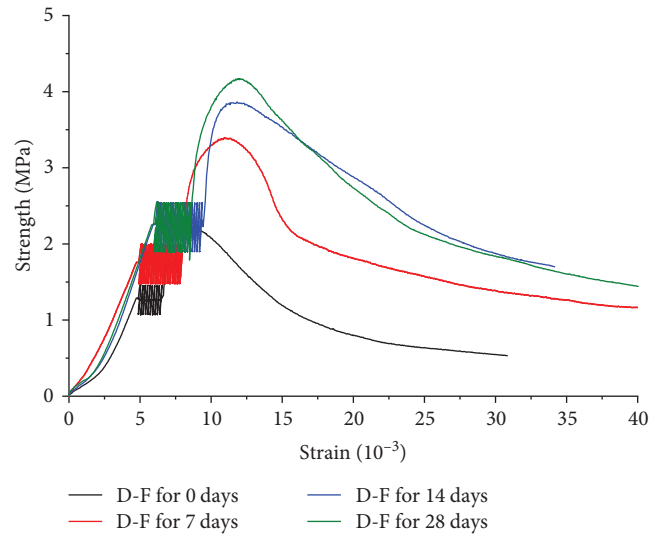
the remaining groups corresponding to the test results showed various trends, including continuously increasing, an initial increase followed by a plateau, an initial increase followed by a decrease and then an increase, and all groups showed no decrease in peak strain overall. Such findings could be attributed to the samples water loss solidification and crystallizing of salts during the natural A-D process. Under such conditions, the gripping force between the soil particles, gels, and fibers was enhanced, so that the samples could still bear large forces without damage under large deformation conditions [40]. The presence of fibers in the specimen under natural A-D conditions resulted in an increase in the peak strain of the sample as its own strength increased. The different trends in peak strain of the specimen during the increase of natural A-D days could be attributed to the different test conditions such as the number of CL, SL, frequency, and so forth. Overall, the peak strain did not decrease with an increase in the number of natural A-D days.

Figure 12 shows that, under the same number of FT cycles, the cumulative strain increased with an increase in peak strain as the number of natural A-D days increased. The maximum cumulative strain corresponding to most test groups occurred after 14 days of natural air drying, with a small number occurring after 7 days of natural air drying. The trend of cumulative strain initially increasing and then decreasing was more pronounced. After continuing the natural A-D process, as the water of the soil evaporated, the salt crystals inside the soil precipitated, which increased the gripping force between the fiber and soil, and limited the deformation of the CL stage. Coupled with the decrease in the strength of the sample after 28 days of natural air drying, the cumulative strain corresponding to the test results of each group showed a decreasing trend.

In summary, the improved saline soil that underwent FT and natural A-D conditions in arid areas maintained high UCS and CL strength. The requirement for the strength of the subgrade base layer was met, which should be greater than 1 MPa according to the *Technical Guidelines for the Construction of*

TABLE 6: Orthogonal test results.

Group	A-D for 0 days			A-D for 7 days			A-D for 14 days			A-D for 28 days		
	σ_p	ε_p	ε_c	σ_p	ε_p	ε_c	σ_p	ε_p	ε_c	σ_p	ε_p	ε_c
1	2.07	6.27	1.127	3.48	10.87	2.520	4.09	12.67	3.035	4.12	12.43	1.87
2	2.42	6.02	1.380	3.22	14.34	3.530	4.80	12.54	2.835	3.71	13.02	2.175
3	2.23	6.95	1.463	3.56	11.69	2.827	3.86	12.31	3.797	3.84	11.96	2.52
4	2.29	6.87	2.353	3.47	13.07	2.740	4.86	12.61	3.090	3.72	11.59	2.07
5	2.20	6.43	0.795	2.74	9.67	1.020	3.51	13.44	1.685	2.88	16.73	1.61
6	2.01	9.13	1.220	2.96	7.69	1.825	3.39	11.84	2.377	3.29	15.28	1.835
7	2.37	7.87	0.930	3.51	9.14	2.070	3.67	14.16	4.370	3.05	16.62	2.685
8	2.05	7.06	1.640	3.20	13.69	4.900	2.80	14.17	7.170	3.55	14.55	3.61
9	2.26	6.49	0.813	3.28	13.28	1.830	3.62	9.86	2.845	3.69	13.00	1.885
10	1.82	7.39	1.560	3.50	15.25	3.515	3.96	11.05	4.650	2.86	13.72	2.82
11	2.02	6.81	1.020	3.27	12.04	1.535	3.55	11.39	1.870	3.14	12.22	1.19
12	2.17	6.52	1.180	3.08	14.06	2.295	3.59	12.86	2.890	3.47	13.74	1.275
13	2.04	5.22	0.537	3.20	10.25	1.890	4.15	11.46	1.700	2.76	16.33	1.54
14	2.36	7.92	0.617	3.07	12.81	1.721	3.15	13.69	1.626	3.07	14.23	1.345
15	2.20	10.84	1.985	3.23	11.96	2.330	3.72	14.84	4.455	3.23	12.24	2.29
16	2.51	8.44	1.271	3.14	14.47	3.250	4.21	14.74	3.790	4.01	14.84	3.25

Highway Road bases (*JTG/T F20-2015*) [34]. Such results indicate that the saline soil improvement scheme is effective and adaptable for use in treating chlorine saline soil in arid areas.

3.3. Range Analysis. The peak strength, peak strain, and cumulative strain range results of improved saline soil samples subjected to different test conditions are shown in Tables 7–9.

Based on the magnitude of the range of peak intensity, the influencing factors on peak intensity could be ranked as follows: LF, FT cycles, CL times, LA, and SLs when natural A-D days were 0 days. After 7 days, the ranking of influencing factors on peak intensity was as follows: FT cycles, SLs, LF, LA, and CL times. After 14 days, the ranking was as follows: FT cycles, SLs, LF, LA, and CL times. After 28 days, the ranking was as follows: FT cycles, SLs, CL times, LF, and LA. An observation can be made that the FT number and SL had significant effects on the strength of improved saline soil, while the regularity of other influencing factors was not significant. Such observation is consistent with the results presented in Figure 9.

According to the magnitude of the peak strain range, the influencing factors on the peak intensity could be ranked as follows: LA, CL times, FT cycles, LF, and SL when the natural A-D days were 0 days. At 7 days, the ranking was as follows: FT cycles, CL times, LF, SL, and LA. At 14 days, the ranking was as follows: FT cycles, CL times, SL, LF, and LA. At 28 days, the ranking was as follows: FT cycles, CL times, LA, LF, and SL. With the increase in the number of natural A-D days, and in combination with the findings from Figure 11, it can be observed that the number of FT times and CL times had a significant effect on the deformation of improved saline soil, while the impact of other influencing factors was not significant.

According to the magnitude of the cumulative strain range, the influencing factors on the cumulative strain could be ranked as follows: when the natural A-D days were 0 days, CL times, LA, LF, SL, and the number of FT cycles. At 7 days, the ranking was as follows: LF, CL times, LA, FT cycles, and SL. At 14 days, the ranking was as follows: LF, CL times, SL, FT cycles, and LA. At 28 days, the ranking was as follows: LF, CL times, LA, FT cycles, and SL. With the increase in the number of natural A-D, combined with Figure 12, the LF and CL times had significant effects on the cumulative deformation of improved saline soil, while the regularity of other influencing factors was not significant.

3.4. Specimen Morphological Analysis. Through observation of the CL test for sample destruction (G12-7 refers to the test where the sample was destructed after 7 days of natural A-D in group 12, and the other tests were not repeated), the failed samples from the 12th group of CL tests were selected. As depicted in Figure 13(a)–13(d), the surface salt analysis significantly increased with the increase in natural A-D days, resulting in the appearance of peeling, shedding, and other salt expansion phenomena on the surface. The failure form remained consistent, and complete penetrating cracks did not appear. CL test samples that underwent natural A-D for 28 days were chosen for analysis, as presented in Figure 13 (e)–13(h). It was observed that with an increase in FT times under identical natural A-D days, the surface salt analysis of the sample significantly increased, and penetrating cracks gradually manifested. The cyclic load exerted at the top of the specimen caused the cracks to appear from the top, with the upper portion of the specimen being more severely damaged than the bottom end.

4. Microstructure Analysis

Natural saline soil samples (Figures 14(a) and 14(b)), improved saline soil (Figures 14(c) and 14(d)), samples that underwent different days of natural A-D at the same number of FT cycles (Figure 14(e)–14(h)) and samples with different FT cycles
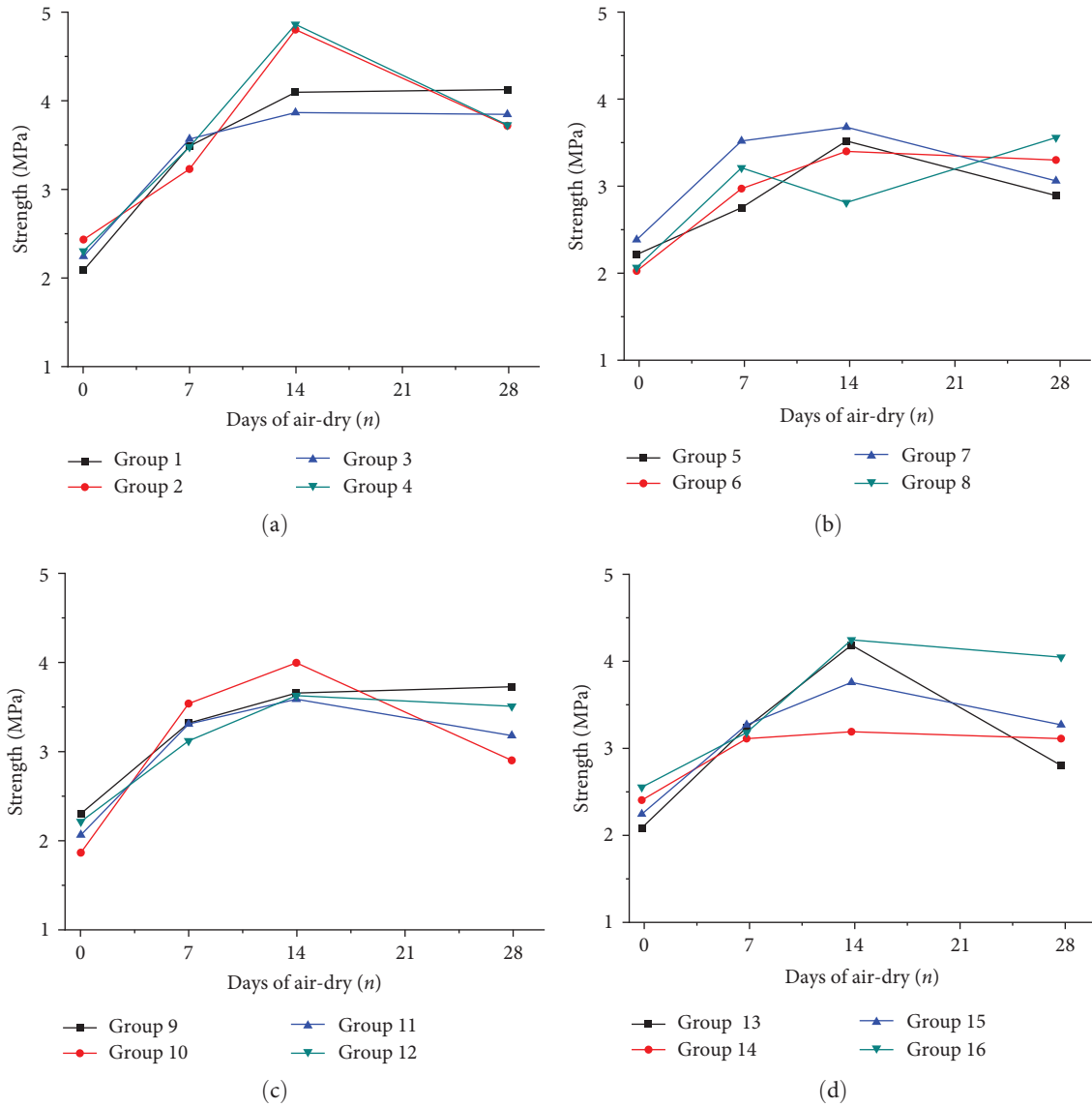
FIGURE 10: Curves of intensity and natural air-drying days.

under 28 days natural A-D conditions (Figure 14(i)–14(l)) were selected and the morphology, connection mode, salt crystallization, and pore development of mineral particles were observed at 4,000 times, as shown in Figure 14.

The XRD test results of natural saline soil powder were analyzed (see Figure 15), and the main components of natural saline soil were found to be Quartz SiO_2 at 23.2%, Mica $KAl_2(AlSi_3O_{10})(OH)_2$ at 29.1%, Dolomite $CaMg(CO_3)_2$ at 10.5%, and Albite $Na(AlSi_3O_8)$ at 10%. Combined with Figures 14(a) and 14(b), the salt distribution of saline soil in the natural state appeared to be uneven, with most of the mineral particles being small, different in size, and the distribution being scattered and fragmented. In the salt-free crystallization area, the contact mode between particles was point–point–surface contact, and the microstructure was relatively loose.

EDS surface analysis was performed on the rectangular labeled cementation area in Figure 14(b), revealing that the fluid-like gel consisted of three elements: Cl, Na, and O, with mass percentage contents of 49.73%, 40.08%, and 10.19%, respectively. It can be inferred that the gel was a sodium chloride crystal. In the sodium chloride crystal area, the gel evidently had a mirror-like appearance, with the gaps between the particles filled by sodium chloride crystal. Most of the small particles were wrapped by the crystal, with almost no porosity present. The contact mode between the particles was mainly point–surface–surface contact, and the microstructure was relatively dense. Due to the limited salt content, resulting in uneven salt distribution, most of the microstructure of the area was obviously loose, and the rest of the area was filled with sodium chloride crystals, which were relatively dense. However, sodium chloride crystals are water-soluble, which can cause natural saline soil to collapse and reduce its compressive strength under certain water conditions. On the other hand, natural A-D leads to soil water loss, resulting in the recrystallization of sodium chloride to fill the pores, which gives
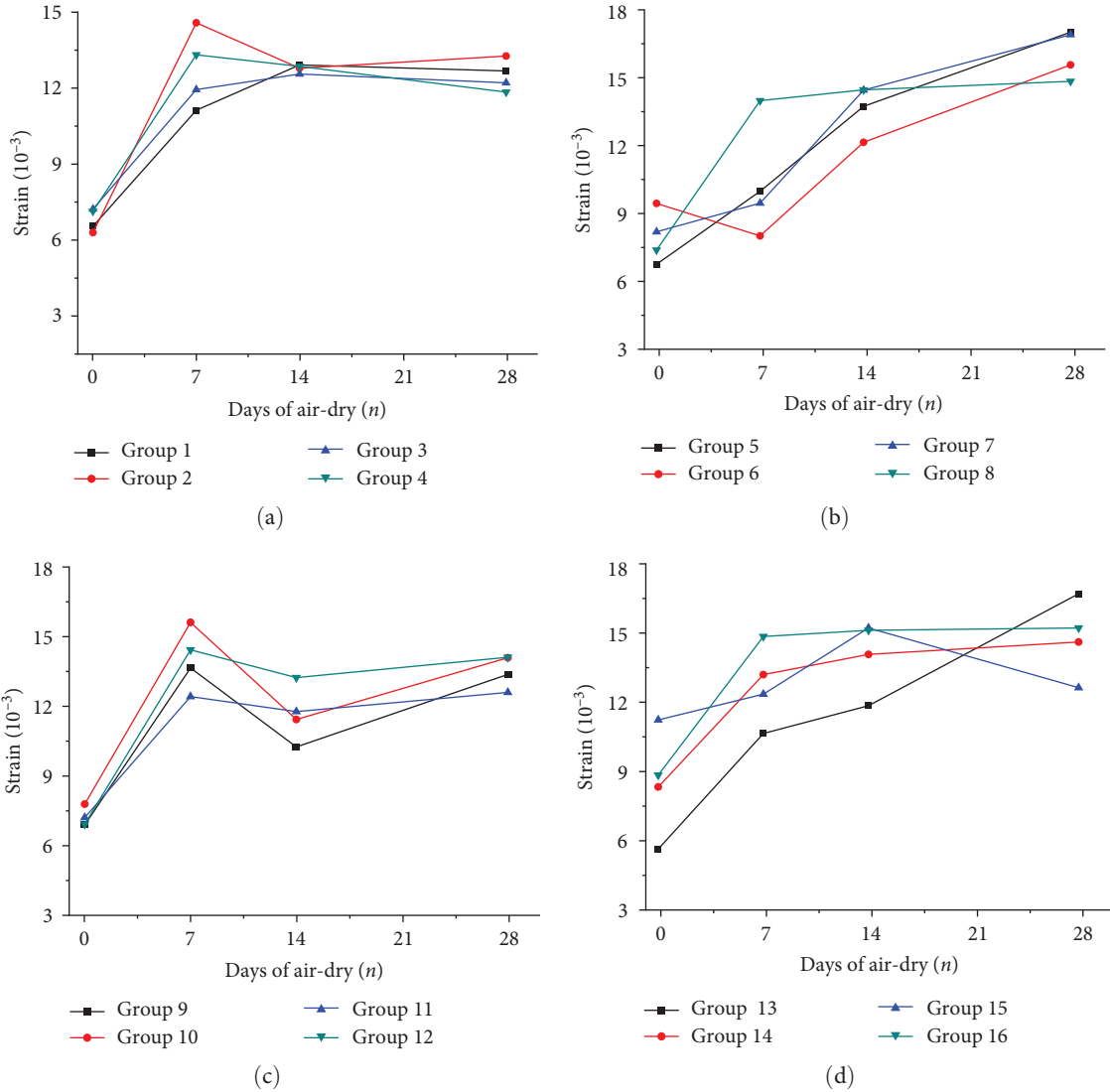
FIGURE 11: Curves of peak strain and natural air-drying days.

the saline soil a certain strength but also alters the internal soil structure, leading to poor engineering geological properties.

The XRD diffraction pattern of the improved saline soil powder is presented in Figure 16, which indicates that the major components are Quartz SiO_2 (23.2%), Mica $KAl_2(AlSi_3O_{10})(OH)_2$ (24.7%), and Calcium carbonate $CaCO_3$ (28.2%). In addition, the EDS surface scan of the rectangular labeled area in Figure 14(c) revealed that the flocculent cement was primarily composed of elements O, Si, and Ca, with mass percentage contents of 56.25%, 16.51%, and 15.17%, respectively. Based on such composition, it could be inferred that the flocculent gel was hydrated calcium silicate. The analysis of the marked area of Figure 14(d) shows that the needle-like gel was composed of O, Ca, C, and three other elements, with percentage contents of 45.15%, 16.92%, and 37.93%, respectively. The gel could be inferred to be calcium carbonate. From Figures 14(c) to 14(d), the improved saline soil mineral particles were generally large, lumpy, or flaky, and the small pores between the particles were filled by the gel. At the same time, there were still some

pores that were not filled by the gel. The contact mode between particles was point–surface–surface contact, and the presence of gel rendered the microstructure denser than that of natural saline soil.

Figure 14(e)–14(h) are SEM diagrams of the 12th group specimen under natural A-D conditions of 0, 7, 14, and 28 days, and at the same number of FT cycles, with the increase in the natural A-D times, the gel increased significantly, the pores were filled, and the microscopic results became increasingly denser overall. Figure 14(i)–14(l) are SEM diagrams of samples that underwent natural A-D for 28 days after 0, 2, 4, and 6 FT cycles. Findings were made that the distribution of flocculent and needle-like gels was more obvious, and under the same natural A-D days, with the increase in FT times, the pores between particles gradually increased, and a large number of micropores and small particles appeared, with their microstructure becoming less dense.

4.1. Analysis of Improvement Mechanism. The XRD analysis of the soil samples is presented in Figure 17, which reveals
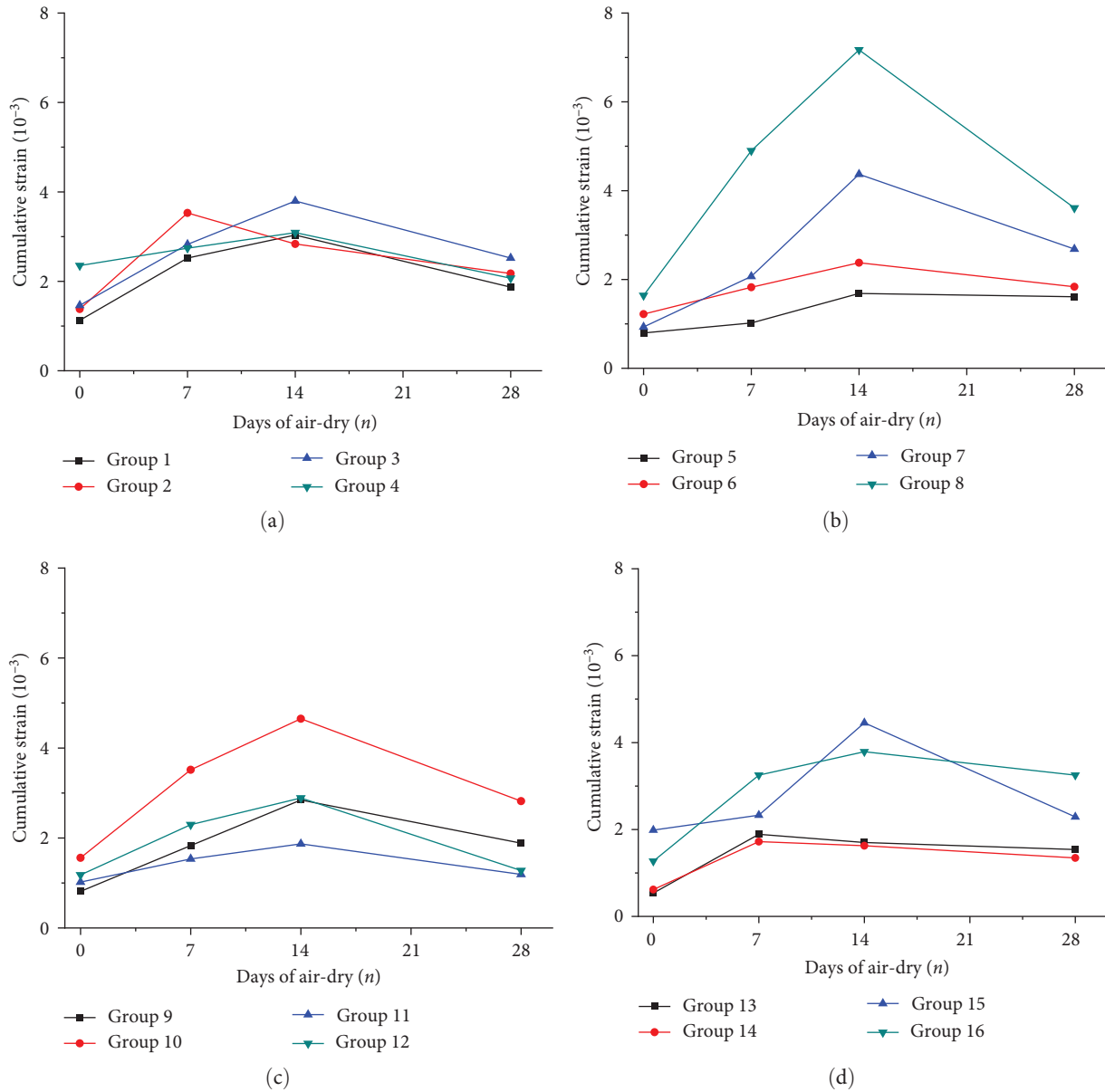
(a)

(b)

(c)

(d)

FIGURE 12: Curves of cumulative strain and natural air-drying days.

TABLE 7: Peak strength σ_p range analysis.

A-D (n)	FT (n)	CL (n)	SL (%)	LA (%)	LF (Hz)
0	0.21	0.165	0.095	0.109	0.355
7	0.43	0.218	0.352	0.273	0.309
14	1.059	0.165	0.802	0.273	0.432
28	0.656	0.456	0.543	0.192	0.412

TABLE 9: Cumulative strain ε_c range analysis.

A-D (n)	FT (n)	CL (n)	SL (%)	LA (%)	LF (Hz)
0	0.065	1.043	0.436	0.879	0.479
7	0.610	1.481	0.538	0.813	1.562
14	1.011	1.794	1.092	0.739	2.871
28	0.643	0.825	0.502	0.756	1.093

TABLE 8: Peak strain ε_p range analysis.

A-D (n)	FT (n)	CL (n)	SL (%)	LA (%)	LF (Hz)
0	1.578	2.015	0.825	2.055	0.935
7	3.611	2.804	1.599	1.27	2.021
14	2.392	1.738	1.100	1.057	1.066
28	3.545	1.362	1.13	1.286	1.135

the main components to be Quartz SiO_2 (22.4%), Calcium carbonate $CaCO_3$ (10.5%), Dolomite $CaMg(CO_3)_2$ (7.9%), Albite $Na(AlSi_3O_8)$ (10.9%), Potassium feldspar $K(AlSi_3O_8)$ (4.4%), Gypsum $CaSO_4(H_2O)_2$ (9.2%), Chlorite $(Mg, Al)_6(Si, Al)_4O_{10}(OH)_8$ (8.6%), and Mica $KAl_2 (AlSi_3O_{10}) (OH)_2$ (26.2%). From the above microstructure analysis, the original components of the plain soil and inorganic materials such as

FIGURE 13: Comparison of the failure morphology of the specimen. (a) G12-0, (b) G12-7, (c) G12-14, (d) G12-28, (e) G4-28, (f) G8-28, (g) G12-28, and (h) G16-28.

sodium chloride, cement, lime, and water glass form hydrostatic gels and gas hard gels under hydration and natural A-D conditions, filling the pores of the soil and improving the strength of the soil. Based on the above XRD and SEM result analysis, Figure 18 shows a general schematic diagram of probable interactions in improved chlorine saline soil. Physical and chemical reactions in improved chlorine saline soil are illustrated as follows:

4.2. The Formation of Water-Hard Gels.

Combined with the SEM images, EDS analysis was performed on water-hard gels, as shown in Figure 19 in the rectangular labeled area. The gels were composed of O, Ca, S, Si, Al, and other elements, with mass percentages of 61.81%, 19.17%, 7.30%, 6.25%, and 5.47%, respectively. It can be inferred that NaOH and $Ca(OH)_2$ produced by the hydrolysis of water glass and quicklime provided an alkaline environment in

the soil, and SiO_2 in the water glass and soil was activated to promote cement hydration and form $CaO \cdot SiO_2 \cdot H_2O$ gel (CSH) [41, 42]. The formation process was as follows Equations (2)–(4). Next, Al_2O_3 in cement was activated in an alkaline environment and reacted with $Ca(OH)_2$ to form $CaO \cdot Al_2O_3 \cdot H_2O$ gel (CAH), the formation process of which was as follows Equation (5). CAH gel further produced sulfate ions with gypsum powder $CaSO_4$ in the soil to form a new $3CaO \cdot Al_2O_3 \cdot 3CaSO_4 \cdot 32H_2O$ gel (AFt), and the formation reaction was as follows Equation (6). The AFt gel present in the soil was observed to have needle-like crystals, and these crystals continued to form during the curing process. As a result, the gels became staggered and overlapped to form a network structure, which filled the pores and connected the soil particles. This network structure contributed to further improvement of the soil's strength [43–45].
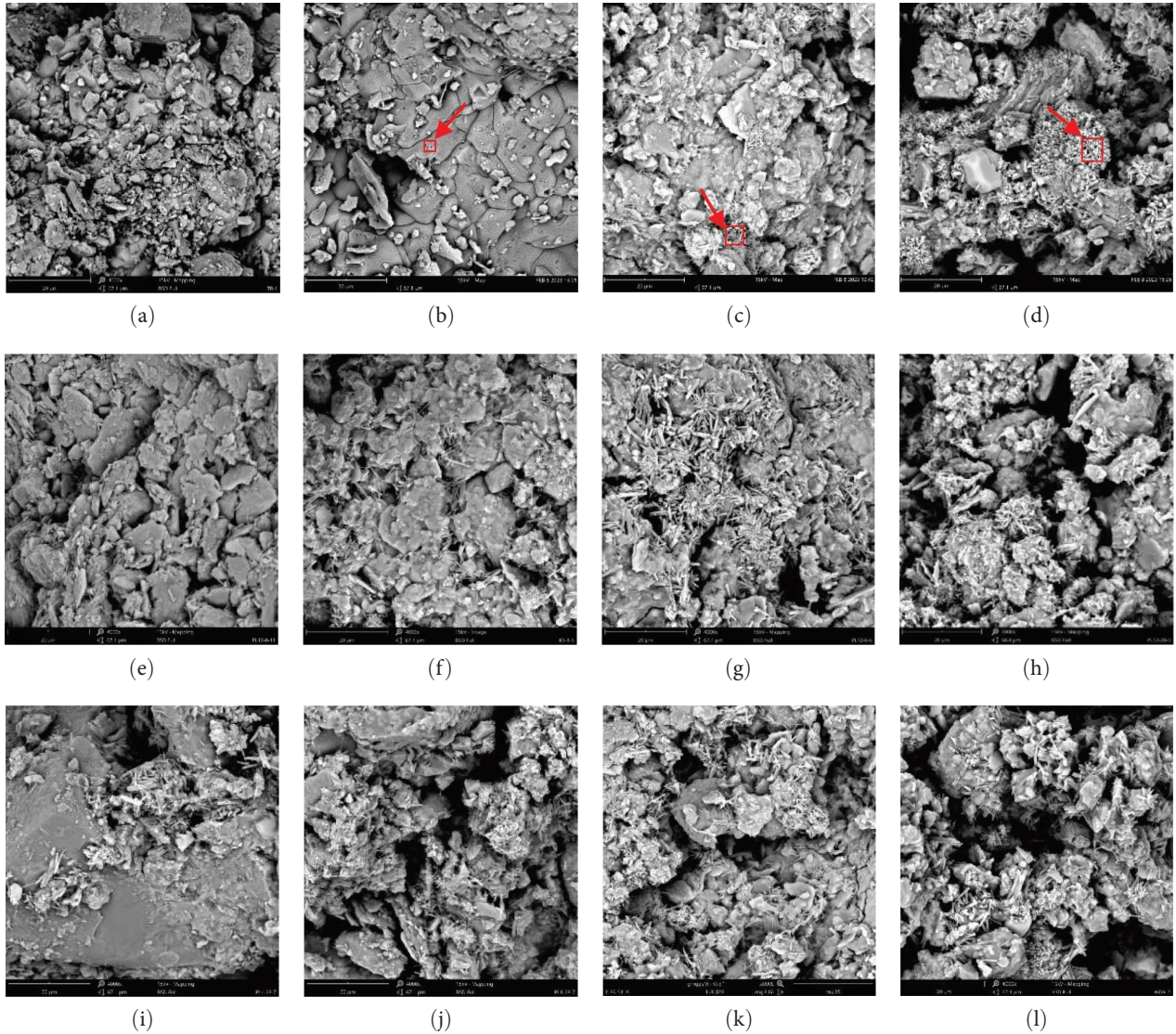
FIGURE 14: SEM diagram of saline soil. (a) Natural saline soil, (b) natural saline soil, (c) improved saline soil, (d) improved saline soil, (e) G12-0, (f) G12-7, (g) G12-14, (h) G12-28, (i) G4-28, (j) G8-28, (k) G12-28, and (l) G16-28.
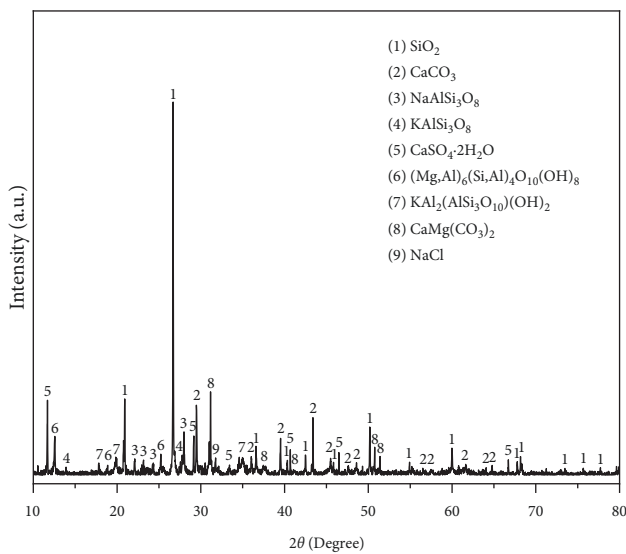
(1) SiO_2
(2) $CaCO_3$
(3) $NaAlSi_3O_8$
(4) $KAlSi_3O_8$
(5) $CaSO_4 \cdot 2H_2O$
(6) $(Mg,Al)_6(Si,Al)_4O_{10}(OH)_8$
(7) $KAl_2(AlSi_3O_{10})(OH)_2$
(8) $CaMg(CO_3)_2$
(9) $NaCl$

FIGURE 15: X-ray powder diffraction pattern of natural saline soil.

(1) SiO_2
(2) $CaCO_3$
(3) $NaAlSi_3O_8$
(4) $KAlSi_3O_8$
(5) $CaSO_4 \cdot 2H_2O$
(6) $(Mg,Al)_6(Si,Al)_4O_{10}(OH)_8$
(7) $KAl_2(AlSi_3O_{10})(OH)_2$
(8) $CaMg(CO_3)_2$
(9) $NaCl$
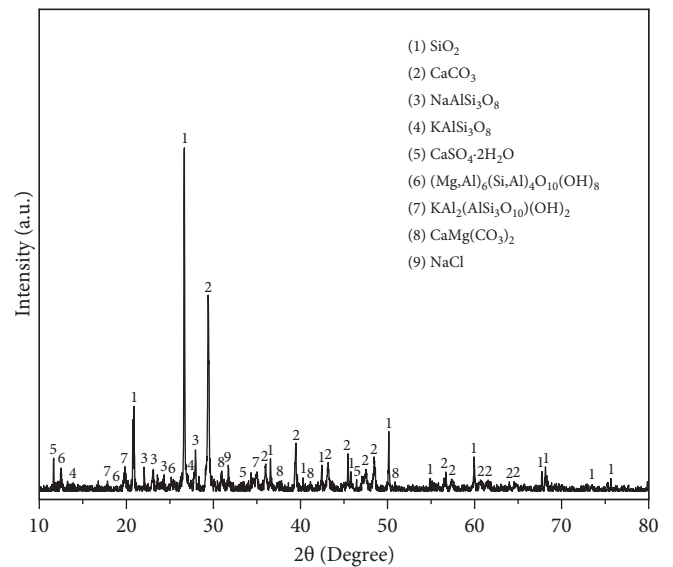
FIGURE 16: X-ray powder diffraction pattern of solidified saline soil.

(1) SiO_2
(2) $CaCO_3$
(3) $NaAlSi_3O_8$
(4) $KAlSi_3O_8$
(5) $CaSO_4 \cdot 2H_2O$
(6) $(Mg,Al)_6(Si,Al)4O_{10}(OH)_8$
(7) $KAl_2(AlSi_3O_{10})(OH)_2$
(8) $CaMg(CO_3)_2$
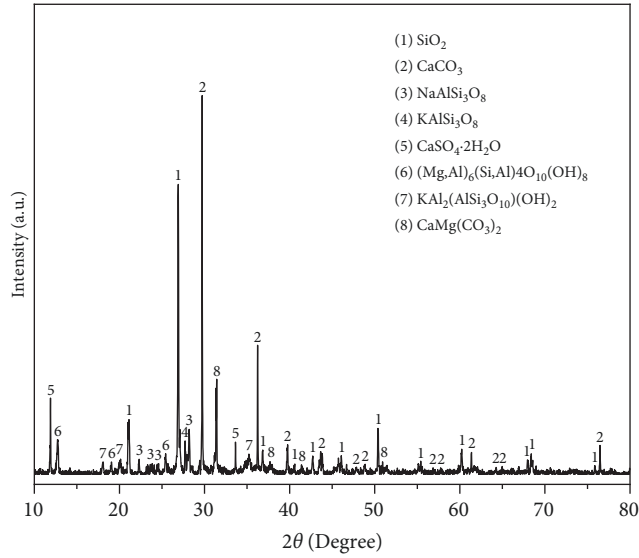
FIGURE 17: X-ray powder diffraction pattern of plain soil.
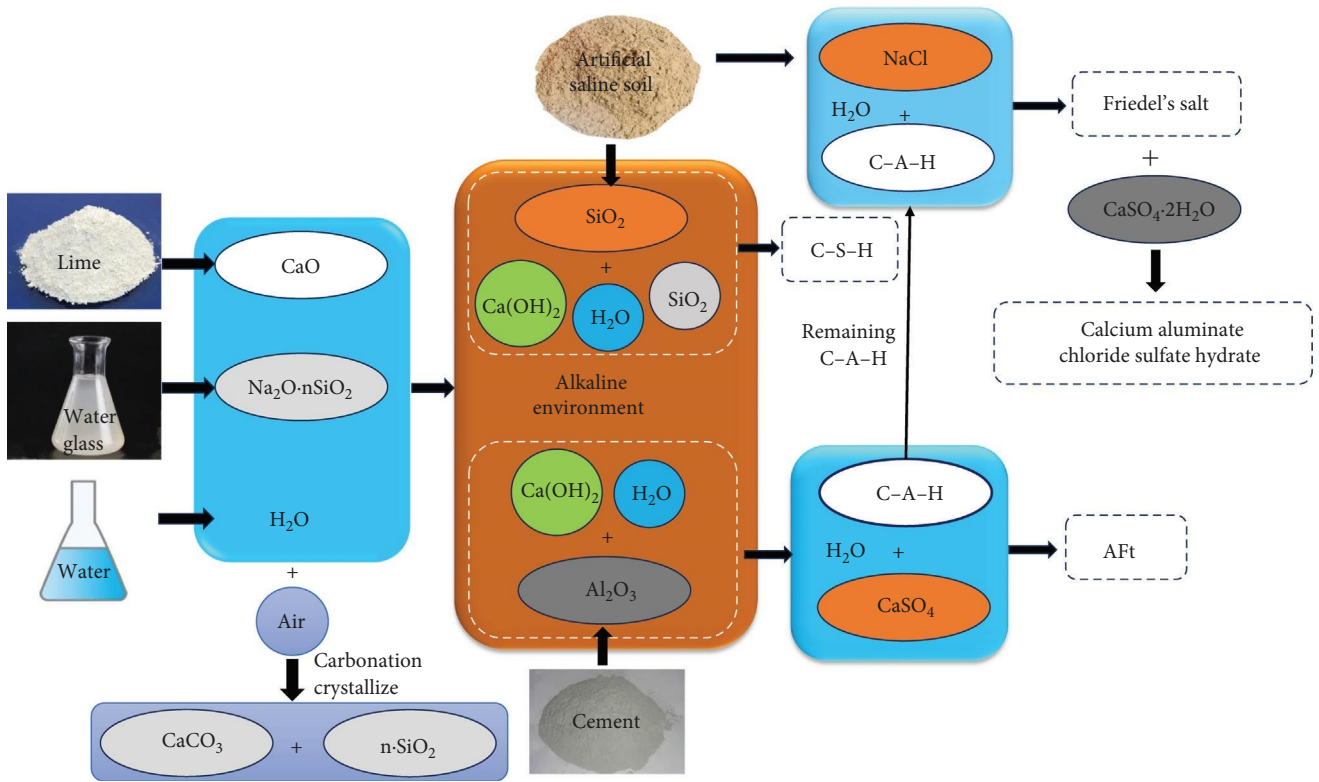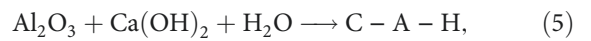

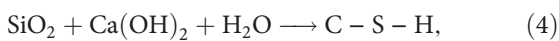FIGURE 18: Schematic diagram of the improvement mechanism.

$$CaO + H_2O \longrightarrow Ca(OH)_2, \qquad (2)$$

$$Na_2O \cdot nSiO_2 + H_2O \longrightarrow 2NaOH + nSiO_2, \qquad (3)$$

$$SiO_2 + Ca(OH)_2 + H_2O \longrightarrow C-S-H, \qquad (4)$$

$$Al_2O_3 + Ca(OH)_2 + H_2O \longrightarrow C-A-H, \qquad (5)$$

$$CaO \cdot Al_2O_3 \cdot H_2O + CaSO_4 + H_2O \longrightarrow AFt. \qquad (6)$$
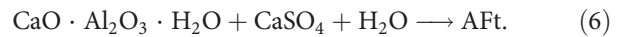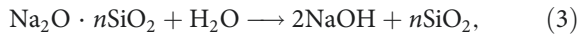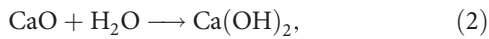
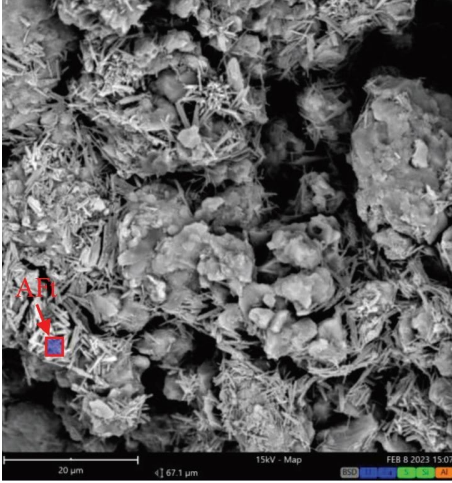Due to the limited content of $CaSO_4$ in saline soil and inorganic materials, part of the CAH combined with sulfate
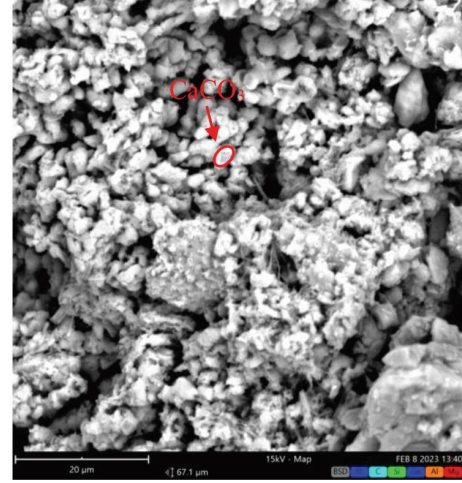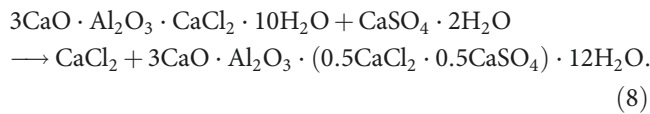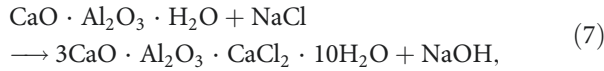
FIGURE 19: SEM diagram of hydrostatic gel.
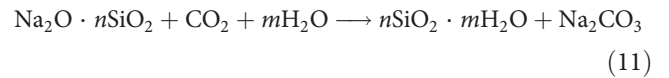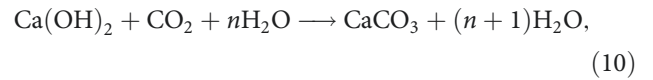

FIGURE 20: SEM diagram of aero rigid gel.

ions to form AFt, and the remaining CAH reacted with Cl^- in saline soil to generate $3CaO \cdot Al_2O_3 \cdot CaCl_2 \cdot 10H_2O$ [46]. The formation reaction was as follows Equation (7). In the environment where sulfate ions were partially enriched, sulfate ions continued to replace part of the chloride ions in $3CaO \cdot Al_2O_3 \cdot CaCl_2 \cdot 10H_2O$ formed calcium aluminate hydrate [5]. The formation process was as follows Equation (8). The process consumed soluble chloride ions in the improved saline soil, thereby improving the engineering characteristics of the solidified saline soil to a certain extent.

$$CaO \cdot Al_2O_3 \cdot H_2O + NaCl \longrightarrow 3CaO \cdot Al_2O_3 \cdot CaCl_2 \cdot 10H_2O + NaOH, \quad (7)$$

$$3CaO \cdot Al_2O_3 \cdot CaCl_2 \cdot 10H_2O + CaSO_4 \cdot 2H_2O \longrightarrow CaCl_2 + 3CaO \cdot Al_2O_3 \cdot (0.5CaCl_2 \cdot 0.5CaSO_4) \cdot 12H_2O. \quad (8)$$

4.3. The Formation of Gas Rigid Gels. The gas rigid gels shown in the annotated areas of Figure 20 were analyzed using SEM images and EDS analysis, revealing that the gels were composed of elements such as O, C, Si, Ca, Al, and Mg. The mass percentages of the elements were found to be 54.19%, 24.59%, 7.47%, 9.50%, 2.49%, and 1.77%, respectively. It can be inferred that as the sample naturally dried, the $Ca(OH)_2$ formed by lime hydrolysis in the soil sample underwent a transformation from a colloidal to a crystalline state during the process of dry hardening. At the same time, $Ca(OH)_2$ carbonized with CO_2 in the air to form $CaCO_3$ [47], and the formation process was as follows Equations (9) and (10). As the sample is naturally A-D, the water glass is carbonized with CO_2 in the air to form a silicate gel. During the process of dehydration and crystallization, the gel was further consolidated, forming a more solid structure. The formation process was as follows Equation (11). Therefore, the gas rigid gels were mainly solid SiO_2 and calcium carbonate.

$$CaO + H_2O \longrightarrow Ca(OH)_2, \quad (9)$$

$$Ca(OH)_2 + CO_2 + nH_2O \longrightarrow CaCO_3 + (n+1)H_2O, \quad (10)$$

$$Na_2O \cdot nSiO_2 + CO_2 + mH_2O \longrightarrow nSiO_2 \cdot mH_2O + Na_2CO_3 \quad (11)$$

5. Conclusion

In order to use in situ saline soil to treat the subgrade, the optimal ratio of chlorine saline soil suitable for treating subgrade in arid areas was investigated. The main findings of the present investigation are as follows:

(1) The chlorine saline soil with a salt content of 3% can be used for subgrade treatment in arid areas when the optimal values for cement content, lime content, fiber content, and fiber length are 8%, 12%, 0.2%, and 18 mm, respectively.

(2) With the increase in FT cycles, the UCS of the optimal ratio sample gradually decreased. Under the same number of FT cycles, with the increase of natural A-D days, there was a trend of first increasing and then decreasing in the UCS.

(3) According to the results of C-L testing, with the increase of natural A-D times, the FT number, and SL were the main factors affecting the strength; the number of FT times and the number of cycles were the main factors affecting the deformation; and the frequency and cycle number were the main factors affecting the cumulative deformation. The fiber was mixed so that the improved saline soil after destruction could still maintain a high compressive strength value.

(4) The mechanism of inorganic material improvement of saline soil is essentially related to the formation of

water-hard gels such as CSH, AFt, and calcium aluminate hydrate in the standard curing 28 days process, and gas rigid gels such as solid SiO_2 and calcium carbonate formed by the loss of water in soil samples under natural A-D conditions. The formation of these gels is the primary factor responsible for improving the strength and deformation performance of the improved saline soil.

The improved saline soil that underwent FT and natural A-D conditions in arid areas maintained high UCS and CL strength. The above optimally improved ratio is effective and adaptable for use in treating chlorine saline soil in arid areas. Future research should focus on the long-term water–salt migration and salt crystallization effects on the improvement mechanism of inorganic materials in saline soil and the strength properties of improved saline soil, especially if the salt content exceeds 3%. This will require further study to verify the applicability of the above research results.

Data Availability

The data used to support the findings of this study are included within the article.

Conflicts of Interest

The authors declare that they have no conflicts of interest.

Authors' Contributions

Semaierjiang Maimaitiyusupu and Cheng Zhao contributed equally as cofirst authors.

Acknowledgments

References

[1] L. Q. Wen, *Origin and Distribution Characteristics of Saline Soil in China*, Hefei University of Technology, (in Chinese), 2010.

[2] X. R. Niu, Z. N. Li, and J. P. Gao, "Study progress in salt expansion characteristic and mechanism of saline soil," *Chinese Journal of Soil Science*, vol. 39, no. 1, pp. 163–168, (in Chinese), 2008.

[3] G. Rajasekaran, "Sulphate attack and ettringite formation in the lime and cement stabilized marine clays," *Ocean Engineering*, vol. 32, no. 8-9, pp. 1133–1159, 2005.

[4] Y. Cheng, H. Yu, B.-L. Zhu, and D.-X. Wei, "Laboratory investigation of the strength development of alkali-activated slag-stabilized chloride saline soil," *Journal of Zhejiang University-Science A*, vol. 17, no. 5, pp. 389–398, 2016.

[5] Y. Shen, P. Li, P. Jing, Y. Liu, R. Feng, and X. Liu, "Experiment and mechanism analysis on the solidification of saline dredger fill with composite slag solidifying agent: a case study in Caofeidian, China," *Applied Sciences*, vol. 12, no. 4, Article ID 1849, 2022.

[6] C. B. Liu, H. G. Ji, J. H. Liu, W. He, and C. Gao, "Experimental study on slag composite cementitious material for solidifying coastal saline soil," *Journal of Building Materials*, vol. 18, no. 1, pp. 82–87, (in Chinese), 2015.

[7] Y.-H. Qin, F.-H. Liu, and Q. Zhou, "Influencing factors of compressive strength of solidified inshore saline soil using SH lime-ash," *Journal of Central South University of Technology*, vol. 15, no. S1, pp. 386–390, 2008.

[8] C. B. Liu, "Research on strength and microstructure feature of solidified saline soil in inshore with slag cementitious material," *Applied Mechanics and Materials*, vol. 174, pp. 1232–1237, 2012.

[9] Y. Zhu, X. Yu, L. Gao, J. Chen, and M. D. Cotugno, "Unconfined compressive strength of aqueous polymer-modified saline soil," *International Journal of Polymer Science*, vol. 2019, Article ID 9137069, 11 pages, 2019.

[10] Y. P. Zhou, Q. F. Guan, and P. Y. Yan, "Investigation of freeze–thaw resistance of stabilized saline soil," *Advances in Civil Engineering*, vol. 2021, Article ID 5555436, 13 pages, 2021.

[11] J.-L. Zhang, Z.-G. Jiang, and G. Yang, "Experimental study on mechanical behaviors of polypropylene fiber reinforced clay," *Chinese Journal of Geotechnical Engineering*, vol. 33, no. S1, pp. 427–432, (in Chinese), 2011.

[12] Q. Wang, *Study on Road Performance of Saline Soil with Lime and Jute Fiber*, Jilin University, (in Chinese), 2019.

[13] X. Yu and Q. Sun, "Experimental research on the strength performance of chlorine saline soil with cement and lime," *Journal of East China Jiaotong University*, vol. 28, no. 5, pp. 29–34, (in Chinese), 2011.

[14] Q. F. LÜ, H. Chen, H. F. Meng, and B. Ma, "Experimental study on the mechanism of modified sodium silicate solidified sulfuric sulphate saline soil," *Subgrade Engineering*, vol. 2, pp. 67–71, (in Chinese), 2018.

[15] Q. F. LÜ, H. F. Meng, S. X. Wang, Q. Zhang, and H. Chen, "Research of strength and freezing–thawing durability of saline soil solidified by modified sodium silicate," *Journal of Beijing University of Technology*, vol. 43, no. 1, pp. 108–112, (in Chinese), 2017.

[16] Q. F. LÜ, G. Zhou, S. X. Wang, Z. S. Huo, and B. Ma, "Microstructure characteristics of solidified saline soil based on nuclear magnetic resonance," *Rock and Soil Mechanics*, vol. 40, no. 1, pp. 245–249, (in Chinese), , 2019.

[17] G. Xing, L. Zhang, W. Xuan, Y. Pan, Y. Zhao, and B. Zhang, "Influence of alkaline activators on unconfined compressive strength of saline soils stabilised with ground granulated blast furnace slags," *Advances in Civil Engineering*, vol. 2021, Article ID 8893106, 13 pages, 2021.

[18] J. N. Wang, L. Huang, C. Y. Wu, and T. Jiang, "Mechanical properties and microstructure of saline soil solidified by alkali-activated steel slag," *Ceramics Silikaty*, vol. 66, no. 3, pp. 339–346, 2022.

[19] S. X. Chai, P. Wang, W. F. Han, F. Li, L. Wei, and X. Y. Wang, "Research on strength and microstructure feature of solidified saline soil in inshore with polymer," *Rock and Soil Mechanics*, vol. 28, no. 6, pp. 1067–1072, (in Chinese), 2007.

[20] S. X. Chai, X. Y. Wang, X. M. Zhong, Y. Guo, P. Wang, and F. Li, "Different salt contents effect on consistency and compactness of saline soil in inshore with lime," *Rock and Soil Mechanics*, vol. 29, no. 11, pp. 3066–3070, (in Chinese), 2008.

[21] S. X. Chai, B. Z. Yang, X. Y. Wang, P. Wang, X. M. Zhong, and L. Wei, "Experimental research on effect of salt content on strength of solidified saline soil in inshore with lime," *Rock and Soil Mechanics*, vol. 29, no. 7, pp. 1769–1772, (in Chinese), 1777, 2008.

[22] S. X. Chai, X. Y. Wang, P. Wang, L. Wei, X. M. Zhong, and F. Li, "Effect of salt content on microstructure indices of solidified inshore saline soil with lime," *Rock and Soil Mechanics*, vol. 30, no. 2, pp. 305–310, (in Chinese), 2009.

[23] S. X. Chai, X. Y. Wang, L. Wei, and P. Wang, "Appreciation of strength and suitability of five solidified saline soils in inshore," *Journal of Liaoning Technical University (Natural Science Edition)*, vol. 28, no. 1, pp. 59–62, (in Chinese), 2009.

[24] L. Wei, S. Chai, Q. Guo, P. Wang, and F. Li, "Mechanical properties and stabilizing mechanism of stabilized saline soils with four stabilizers," *Bulletin of Engineering Geology and the Environment*, vol. 79, no. 10, pp. 5341–5354, 2020.

[25] H. L. Wang, H. J. Chen, S. C. Tang, Z. Y. Hu, and Y. Zhao, "Sand-fixation experimental research of chlorine saline soil in Yardang landform along the railway," *Journal of Railway Science and Engineering*, vol. 14, no. 6, pp. 1199–1205, (in Chinese), 2017.

[26] Y. Z. Wang, Z. H. Li, L. Y. Li, and J. G. Yang, "Experimental research on strength of the cement stabilized oarhan over chlorine saline soil," *Highway*, vol. 61, no. 4, pp. 14–18, (in Chinese), 2016.

[27] Y. M. Wang, L. J. Chang, and Y. Li, "Study on strength characteristics and micro mechanism of saline soil solidified by recycled fine powder of waste concrete," *Material Reports*, vol. 35, no. S2, pp. 268–274, (in Chinese), 2021.

[28] J. Sun, H. Y. Chen, C. Liu, Z. Zhang, Y. L. Li, and X. X. Tian, "Experimental study on curing of ultra-chloride saline soil in arid desertification area," *Journal of Xinyang Normal University Natural Science Edition*, vol. 31, no. 2, pp. 281–285, (in Chinese), 2018.

[29] Ministry of Housing and Urban Rural Development of the People's Republic of China, *Standard for Geotechnical Testing Method (GB/T 50123-2019)*, China Planning Press, Beijing, China, 2019.

[30] A. A. B. Moghal, B. M. Basha, and M. Ashfaq, *Probabilistic Study on the Geotechnical Behavior of Fiber Reinforced Soil, Frontiers in Geotechnical Engineering, Developments in Geotechnical Engineering*, Springer, Singapore, 2019.

[31] A. U. Rehman and A. A. B. Moghal, "The influence and optimization of treatment strategy in enhancing semiarid soil geotechnical properties," *Arabian Journal for Science and Engineering*, vol. 43, no. 10, pp. 5129–5141, 2018.

[32] A. A. B. Moghal, B. C. S. Chittoori, B. M. Basha, and A. M. Al-Mahbashi, "Effect of polypropylene fibre reinforcement on the consolidation, swell and shrinkage behaviour of lime-blended expansive soil," *International Journal of Geotechnical Engineering*, vol. 12, no. 5, pp. 462–471, 2018.

[33] Ministry of Transport of the People's Republic of China, *Fiber for Cement Concrete in Highway (JT/T 524-2019)*, China Communications Press, Beijing, China, 2019.

[34] Ministry of Transport of the People's Republic of China, *Technical Guidelines for the Construction of Highway Roadbases (JTG/T F20-2015)*, China Communications Press, Beijing, China, 2015.

[35] L. Wei, *Fabric Damage and Mechanical Degradation of Coastal Saline Soil Reinforced with Fiber and Lime under Freeze–Thaw Cycling*, Lanzhou University, (in Chinese), 2021.

[36] G. Xing, C. Liu, W. Xuan, Y. Pan, B. Zhang, and Y. Zhao, "Prediction of unconfined compression strength for saline–alkaline soils mixed with cement and wheat straw," *Advances in Materials Science and Engineering*, vol. 2020, Article ID 2765145, 14 pages, 2020.

[37] X. Yu, Y. Wang, and Y. Li, "Stabilization of pavement subgrade soils containing rich chloride salts," *Journal of Transportation Engineering, Part B: Pavements*, vol. 144, no. 3, Article ID 04018025, 2018.

[38] A. A. B. Moghal, B. C. S. Chittoori, B. M. Basha, and M. A. Al-Shamrani, "Target reliability approach to study the effect of fiber reinforcement on UCS behavior of lime treated semiarid soil," *Journal of Materials in Civil Engineering*, vol. 29, no. 6, Article ID 04017014, 2017.

[39] A. A. B. Moghal, B. C. S. Chittoori, and B. M. Basha, "Effect of fibre reinforcement on CBR behaviour of lime-blended expansive soils: reliability approach," *Road Materials and Pavement Design*, vol. 19, no. 3, pp. 690–709, 2018.

[40] N. Khorram and A. M. Rajabi, "Strength properties and microstructural characteristics of clay treated with alkali activated mortar and fiber," *Construction and Building Materials*, vol. 341, Article ID 127486, 2022.

[41] A. Ahmad, M. H. Sutanto, N. R. Ahmad, M. E. Mohamad, and M. Bujang, "Microstructural characterization of fibric peat stabilized with portland cement and silica fume," *Materials*, vol. 16, no. 1, Article ID 18, 2023.

[42] Z. Ren, L. Wang, H. Wang, S. Liu, and M. Liu, "Solidification/stabilization of lead-contaminated soils by phosphogypsum slag-based cementitious materials," *Science of the Total Environment*, vol. 857, no. 3, Article ID 159552, 2023.

[43] J. He, X.-K. Shi, Z.-X. Li, L. Zhang, X.-Y. Feng, and L.-R. Zhou, "Strength properties of dredged soil at high water content treated with soda residue, carbide slag, and ground granulated blast furnace slag," *Construction and Building Materials*, vol. 242, Article ID 118126, 2020.

[44] A. Ahmed and U. H. Issa, "Stability of soft clay soil stabilized with recycled gypsum in a wet environment," *Soils and Foundations*, vol. 54, no. 3, pp. 405–416, 2014.

[45] X. Wang, S. Kim, Y. Wu, Y. Liu, T. Liu, and Y. Wang, "Study on the optimization and performance of GFC soil stabilizer based on response surface methodology in soft soil stabilization," *Soils and Foundations*, vol. 63, no. 2, Article ID 101278, 2023.

[46] A. K. Suryavanshi, J. D. Scantlebury, and S. B. Lyon, "Mechanism of Friedel's salt formation in cements rich in tri-calcium aluminate," *Cement and Concrete Research*, vol. 26, no. 5, pp. 717–727, 1996.

[47] Q. Ma, W. Duan, X. Liu et al., "Engineering performance evaluation of recycled red mud stabilized loessial silt as a sustainable subgrade material," *Materials*, vol. 15, no. 9, Article ID 3391, 2022.